Ultra-Compact Monostatic MIMO Radar with Non-Redundant Aperture

Patrik Grüner, *Graduate Student Member, IEEE,* Martin Geiger, *Graduate Student Member, IEEE,* and Christian Waldschmidt, *Senior Member, IEEE*

***Abstract*—Monostatic multiple-input multiple-output (MIMO) radar configurations using the same antenna array for transmission and reception inherently lead to redundant virtual antenna positions within the virtual MIMO aperture. This paper presents a new method for designing monostatic MIMO radars where this disadvantage may be overcome and non-redundant virtual arrays are yielded by exploiting biomimetic antenna arrays (BMAAs). The new concept of biomimetic MIMO is introduced and thoroughly investigated in this paper. Its working principle is compared to conventional monostatic MIMO and verified by radar measurements. The new approach is intended to improve the angle estimation capability of in particular small radar systems. Therefore, the concept is applied to an ultra-compact two-channel radar monolithic microwave integrated circuit (MMIC) with fully integrated antennas for range and angle measurements in the 150 GHz range. The chip features two monostatic transmit-receive (TRX) channels with an antenna spacing of $\lambda/4$ and occupies less than $3\,\mathrm{mm}^2$ of space. By applying biomimetic MIMO a virtual aperture consisting of four unique antenna positions and an equivalent total size of around 1.5λ is achieved.**

***Index Terms*—biomimetic antenna array (BMAA), biomimetic MIMO, direction-of-arrival estimation (DOA), frequency-modulated continous-wave (FMCW), multiple-input multiple-output (MIMO) radar, radar MMIC, radar-on-chip.**

I. Introduction

THE advancement in semiconductor technology enables the integration of radar sensors on a single chip [1], [2]. The demand for high range resolution and therefore high absolute bandwidth drives the development of radars to higher carrier frequencies. In the frequency range above 100 GHz the antennas become comparatively small, and it is possible to integrate them directly on the monolithic microwave integrated circuit (MMIC). As a consequence, no RF signals have to be routed from or to the MMIC through lossy bond connections. However, if more and more antennas are to be integrated directly on the MMIC to increase the angular resolution of the radar, methods are necessary to limit the required chip area in order to save costs.

Several designs of single-channel frequency-modulated continuous-wave (FMCW) radar sensors above 100 GHz with antennas on chip or in package were presented in the past years [3]–[8]. However, when integrating a complete radar-on-chip, the antennas are typically the largest single components on the MMIC. If an ultra-compact design is desired in order to save expensive chip area, a monostatic design with only one common antenna for transmitting and receiving is therefore preferred [9]–[11].

When it comes to measuring not only distance and velocity but also the angle of a target relative to the radar, at least two receiving channels are required to evaluate the phase progression of the incident plane wave between the antennas. The distance between the respective antennas is of great importance, since a large spacing results in a high angular estimation performance. However, when implementing on an MMIC, the large antenna size as well as the large antenna spacing lead to a significant increase in the chip area, which makes the MMIC more and more expensive. The placement of the antennas off the MMIC on the printed circuit board (PCB), like it is done in [12], [13], should be avoided for frequencies well above 100 GHz since the bond connections introduce high losses and parasitic radiation. If, on the other hand, the antennas are integrated directly on the MMIC, this results in a large chip area [14], [15].

One possible approach to reduce the required chip area is the recently introduced concept of biomimetic antenna arrays (BMAAs). Two antenna elements are coupled in such a way that they mimic the hearing system of the fly *Ormia ochracea* [16]–[19]. The result is a significantly increased angle estimation performance of the antenna array at the expense of a reduction in the signal-to-noise ratio. The BMAA antenna system allows either the enhancement of the angle estimation of an existing antenna array [20] or the spacing between the single antenna elements to be smaller while maintaining the angular performance of the unmodified but larger array.

A method to further increase the angle estimation performance especially in terms of angular separability is to use the radar in a multiple-input multiple-output (MIMO) configuration [21]. A spatial convolution of transmit and receive apertures leads to a virtual aperture being larger than the sum of the TX and RX apertures. However, when combining a MIMO radar system for high angular resolution with the compactness of a monostatic radar system, the resulting virtual MIMO aperture inherently contains redundant virtual antenna positions, which do not deliver additional information. The same holds for bistatic radars if TX and RX antennas are spaced identically [15].

Manuscript received February 5, 2020; revised April 7, 2020; accepted May 29, 2020. This work was funded by the German Research Foundation (DFG, Deutsche Forschungsgemeinschaft) under Grant WA 3506/6-1. *(Corresponding author: Patrik Grüner.)*

The authors are with the Institute of Microwave Engineering, Ulm University, 89081 Ulm, Germany (e-mail: pgruener@ieee.org)

Color versions of one or more of the figures in this paper are available online at https://ieeexplore.ieee.org.

Digital Object Indentifier 10.1109/TMTT.2020.3006055

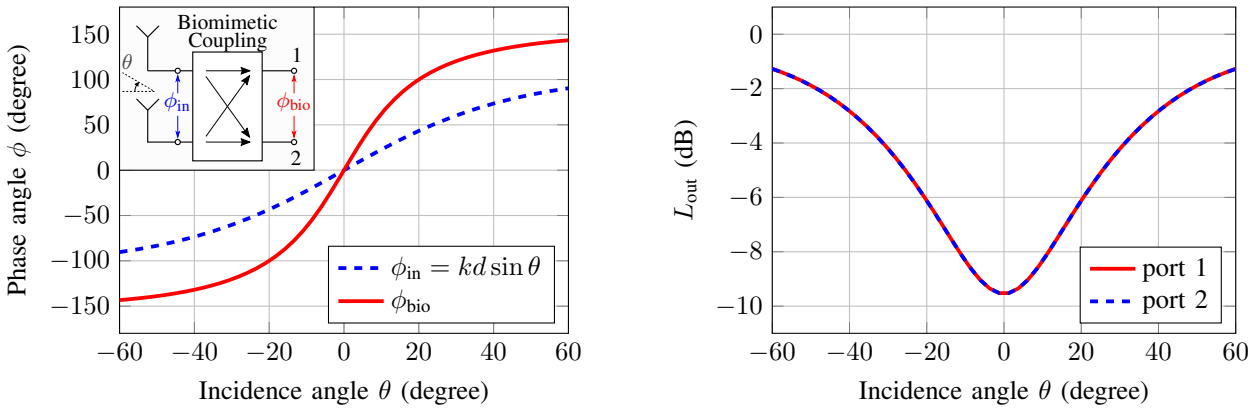

(a) (b)

Fig. 1. Theoretical phase difference curves (a) and output power level L_{out} (b) for a biomimetic antenna array with antenna separation $d = 0.37\lambda$, phase gain $\eta = 3$, and $L_{out} = -9.5$ dB. The two curves for L_{out} are identical and lie on top of each other [18].

This paper presents an ultra-compact two-channel monostatic radar MMIC that enables angular measurements on an extremely small footprint. A fundamentally new MIMO operation is demonstrated by placing the biomimetic coupling of the on-chip biomimetic antenna array only in the receive path of the monostatic radar, which avoids the redundancy of conventional monostatic MIMO arrays, increases the unambiguous angular range, and improves the angular resolution. For the first time, the concept of the BMAA is applied on an MMIC and above 100 GHz in order to reduce the necessary chip area and improve the angle estimation capability. The paper is organized as follows. Section II presents a short summary of the BMAA and introduces the concept of biomimetic MIMO. Section III describes the system design of the ultra-compact two-channel radar MMIC in the 150 GHz range applying the biomimetic MIMO concept. Radar measurements were conducted, and the results are presented in Section IV.

II. Concept of Non-Redundant Monostatic MIMO

A. Biomimetic Antenna Array (BMAA)

In this section, a brief overview of the biomimetic antenna array as a concept to increase the angle estimation performance for electrically small apertures is given. For the sake of compactness, only the effects on a system level are considered and parameters are defined to quantify them. For a detailed explanation of the underlying working principle please refer to [18].

A wave incident from an angle θ leads to a phase progression

$$\phi_{in} = kd \sin\theta := 2\alpha \tag{1}$$

at the antenna terminals of two antennas arranged at a distance d according to the inset in Fig. 1(a), with $k = 2\pi/\lambda$ being the wave number in free space and λ being the wavelength. Due to the biomimetic coupling, the phase difference ϕ_{bio} after the biomimetic coupling network is significantly enlarged compared to ϕ_{in} [18]. An exemplary course of the phase progression is shown in Fig. 1(a). The increased phase sensitivity comes at the cost of a reduction in RX power, which can be extracted from the array (see Fig. 1(b)).

The biomimetic antenna system consisting of two antennas and one coupling network can be fully described on system level by only three parameters: the phase gain η, the off-boresight factor ξ, and the normalized output power L_{out} [18], [22], [23]. The phase gain and the normalized output power compare the BMAA to a regular antenna with the same antenna elements at the same spacing but without the coupling network. The phase gain is defined in boresight direction by normalizing the slope of the phase progression at the terminal of the BMAA (ϕ_{bio}) to the slope of the regular antenna array phase progression (ϕ_{in}):

$$\eta = \frac{\left.\frac{\mathrm{d}\phi_{bio}(\theta)}{\mathrm{d}\theta}\right|_{\theta=0}}{\left.\frac{\mathrm{d}\phi_{in}(\theta)}{\mathrm{d}\theta}\right|_{\theta=0}} . \tag{2}$$

The phase gain basically describes the increase in steepness of the BMAA phase difference compared to the regular antenna array phase difference steepness. The reduction of the output power is quantified by the dimensionless quantity L_{out}:

$$L_{out} = \frac{P_{out,BMAA}}{P_{out,conv.\,Array}} . \tag{3}$$

This value is always less than or equal to 1. The off-boresight factor ξ quantifies the shift in the position of maximum steepness of the phase progression to incidence angles other than boresight (i. e. $|\theta| > 0$) [23]. However, without loss of generality in this paper only boresight BMAAs are assumed and therefore, ξ is always considered as 0.

Based on the introduced BMAA parameters, an analytical expression for the phase difference ϕ_{bio} after the biomimetic coupling can be derived as [17]

$$\phi_{bio} = \arctan\left(\frac{2\eta \tan\alpha}{1 - (\eta^2 + \xi^2)\tan^2\alpha}\right) , \tag{4}$$

with the phase gain η in boresight direction and the off-boresight factor ξ. The corresponding normalized power level calculates to (see Appendix)

$$L_{out} = \frac{\left|1 \pm \mathrm{j}(\eta + \mathrm{j}\xi)\tan\alpha\right|^2}{\left|(\eta + \mathrm{j}\xi) + \mathrm{j}(\eta + \mathrm{j}\xi)\tan\alpha\right|^2} . \tag{5}$$

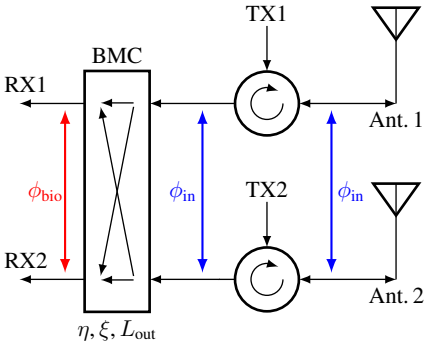

Fig. 2. Monostatic radar system with biomimetic coupling in the receiving path only. ϕ_{in} is the phase difference due to the physical spacing of the antennas, whereas ϕ_{bio} is the phase difference after the biomimetic coupling.

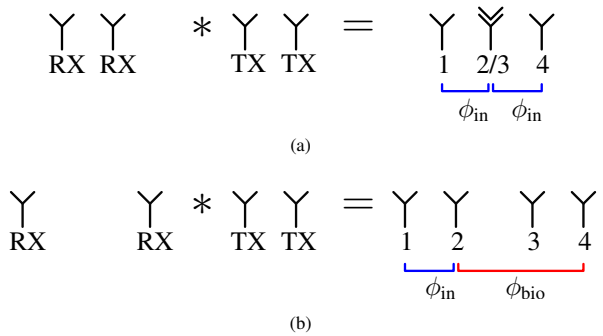

Fig. 3. Formation of the virtual MIMO aperture in boresight direction for (a) a conventional monostatic antenna array and (b) a biomimetic monostatic antenna array with biomimetic coupling in the RX path only.

The course of the phase progression and the output power level in Fig. 1 corresponds to a BMAA with an antenna spacing of $d = 0.37\lambda$, a phase gain of $\eta = 3$, and a minimum normalized power level of $L_{\text{out}} = -9.5\,\text{dB}$.

B. Biomimetic MIMO Antenna System

A well-known method to increase the aperture size is using a radar with multiple transmitters and receivers in multiple-input multiple-output (MIMO) mode [15], [21]. The transmitted signals have to be orthogonal so that they can be distinguished from each other at the receivers. This orthogonality can be established by means of time, frequency, or code multiplexing. If the orthogonality criterion is fulfilled, the antenna apertures of the transmitter and the receiver form a virtual aperture, which is calculated by a spatial convolution of the two apertures [24].

When considering a monostatic radar system with two antennas as it is displayed in Fig. 2, the size of the transmitting (TX) aperture is inevitably identical to the size of the receiving (RX) aperture as the very same antennas are used. As a consequence, the array steering vectors in both cases are identical and can be modeled by

$$\boldsymbol{a}_{\text{RX}}(\theta) = \boldsymbol{a}_{\text{TX}}(\theta) = \left(1, \quad \mathrm{e}^{-\mathrm{j}\phi_{\text{in}}}\right)^{\mathrm{T}}. \tag{6}$$

Each element of the steering vector is normalized to the first array element. The resulting steering vector of the virtual array in the monostatic MIMO case is given by

$$\boldsymbol{a}(\theta) = \left(1, \quad \mathrm{e}^{-\mathrm{j}\phi_{\text{in}}}, \quad \mathrm{e}^{-\mathrm{j}\phi_{\text{in}}}, \quad \mathrm{e}^{-\mathrm{j}2\phi_{\text{in}}}\right)^{\mathrm{T}}, \tag{7}$$

where $\boldsymbol{a}(\theta) = \boldsymbol{a}_{\text{TX}}(\theta) \otimes \boldsymbol{a}_{\text{RX}}(\theta)$ is the Kronecker product of the steering vectors of the transmitter (TX) and the receiver (RX) aperture [24]. While the steering vector consists of four entries, the actual virtual aperture consists of only three elements because one element is redundant and does not deliver additional information. The transmitter and receiver apertures as well as the resulting virtual aperture with the redundant element are depicted in Fig. 3(a).

By comparing the phase progressions of biomimetic and conventional arrays in Fig. 1 the steeper phase progression in the biomimetic case may be regarded as a larger antenna element spacing. This enables a fundamentally new architecture for monostatic MIMO radar systems. By using the biomimetic coupling (BMC) only in the receiving path of the radar, the RX aperture seems to be larger compared to the TX aperture. Mathematically, the steering vectors in the TX and RX are

$$\boldsymbol{a}_{\text{TX}}(\theta) = \left(1, \quad \mathrm{e}^{-\mathrm{j}\phi_{\text{in}}}\right)^{\mathrm{T}} \tag{8}$$

$$\boldsymbol{a}_{\text{RX,bio}}(\theta) = \left(1, \quad \mathrm{e}^{-\mathrm{j}\phi_{\text{bio}}}\right)^{\mathrm{T}}. \tag{9}$$

The resulting virtual array steering vector for the MIMO operation, normalized to the first array element, is then given by

$$\boldsymbol{a}_{\text{bio}}(\theta) = \left(1, \quad \mathrm{e}^{-\mathrm{j}\phi_{\text{bio}}}, \quad \mathrm{e}^{-\mathrm{j}\phi_{\text{in}}}, \quad \mathrm{e}^{-\mathrm{j}(\phi_{\text{in}}+\phi_{\text{bio}})}\right)^{\mathrm{T}}, \tag{10}$$

where $\boldsymbol{a}_{\text{bio}}(\theta) = \boldsymbol{a}_{\text{TX}}(\theta) \otimes \boldsymbol{a}_{\text{RX,bio}}(\theta)$. The resulting virtual aperture no longer contains redundant elements but four individually placed virtual antenna elements. The BMAA principle allows the scaling of the RX aperture while the physical separation of the two antenna elements remains constant. As a consequence, the virtual array is built up of four virtual antenna elements, while only two physical antenna elements are necessary. The principle and the resulting virtual aperture are illustrated in Fig. 3(b).

The antenna system performance is evaluated by the ambiguity function (AF) defined as follows by [25]

$$\text{AF}(\theta_i, \theta_j) = \frac{\boldsymbol{a}(\theta_i)^{\mathrm{H}} \cdot \boldsymbol{a}(\theta_j)}{\left\|\boldsymbol{a}(\theta_i)\right\| \left\|\boldsymbol{a}(\theta_j)\right\|}, \tag{11}$$

where $(\cdot)^{\mathrm{H}}$ denotes the Hermitian operator and $\|\cdot\|$ the Euclidean norm of a vector. The AF is a measure of how similar the steering vectors are for two incidence angles θ_i and θ_j and takes values between 0 and 1. Fig. 4(a) shows the ambiguity function of the conventional antenna array according to the virtual array steering vector in (7), whereas Fig. 4(b) shows the same for the system with biomimetic coupling with a phase gain of $\eta = 3$ in the RX path according to (10). A physical antenna spacing of $d = 0.37\lambda$ was assumed in both cases. A significantly narrower main lobe around the boresight direction ($\theta_i = 0°$) due to the enlarged aperture can be recognized ($\theta_{3\,\text{dB,BMAA}} = 29°$ vs. $\theta_{3\,\text{dB,conv}} = 58°$). The peak phase gain is established in boresight direction but decays with increasing incidence angle θ. As a consequence, no ambiguity occurs.

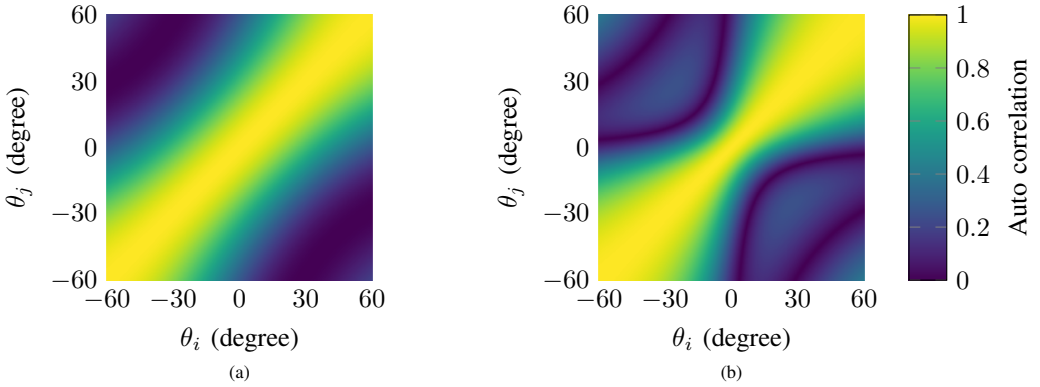

Fig. 4. Absolute value of the ambiguity function (AF) of (a) the conventional, redundant virtual array and (b) the biomimetic, non-redundant virtual array according to Fig. 3 with physical antenna element spacing of $d = 0.37\lambda$.

For very large incidence angles ($\theta \to 90°$), both patterns are similar because the phase gain reduces to around 1.

III. Radar MMIC System Design

The objective of this work was to show that biomimetic MIMO not only prevents redundant elements in the virtual aperture but also leads to very compact radar systems. An MMIC was developed in order to verify the principle of biomimetic MIMO. The concepts applied in the radar system design are described in this section.

A. Radar System Concept

As the antennas are usually the largest single components on an MMIC, it is desired to reduce their number to a minimum. Consequently, the presented MMIC is designed as a monostatic radar so that only one antenna is required for each of the two channels. The necessary transmit-receive coupler (TRC) is realized as an extremely compact rat-race coupler with one port terminated by $50\,\Omega$, see [11]. With its outer dimensions of $140\,\mu\text{m} \times 110\,\mu\text{m}$ the transmit-receive coupler only occupies approx. 10% of the area of an additional antenna, justifying the choice of the monostatic setup in order to be as compact as possible.

A simplified block diagram of the realized MMIC is depicted in Fig. 5. The building blocks of the MMIC presented in this work are in parts based on the works in [11], [26]. The MMIC incorporates an on-chip push-push type VCO operating in the frequency range around $59\,\text{GHz}$ and is stabilized by an on-chip integer-N PLL (see block "fixed-frequency PLL" in Fig. 5). As a reference frequency for the PLL a signal in the frequency range of $920\,\text{MHz}$ has to be fed to the MMIC. The signal of the on-chip VCO is doubled in frequency and used to up-mix an FMCW ramp signal. This FMCW ramp signal, which has to be generated off-chip has a center frequency of around $9\,\text{GHz}$ and its frequency is multiplied by a factor of four on-chip before up-mixing. The signal generation forms an offset synthesizer with a low multiplication factor and is therefore optimized for low phase noise [4].

The synthesized signal in the $150\,\text{GHz}$ range is then divided into the two channels by an active power splitter (PS). In each

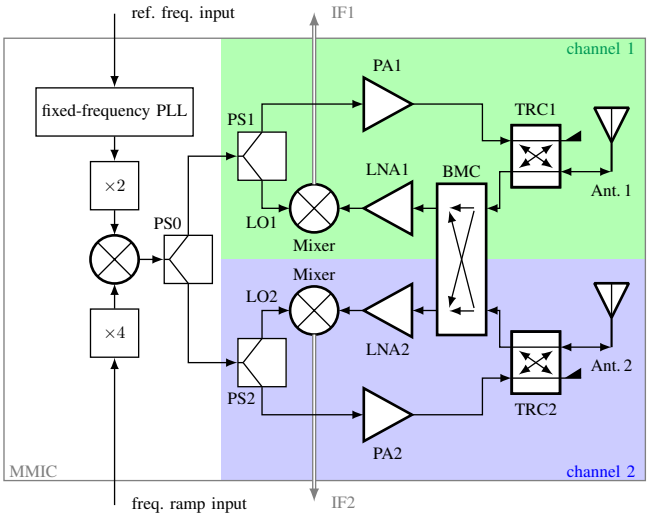

Fig. 5. Block diagram of the presented MMIC. Components belonging to channel 1 are highlighted in green, whereas channel 2 is marked in blue.

channel, the signal is divided once again by the same type of power splitter into the transmit signal and the local oscillator (LO) signal. In the transmit path a power amplifier (PA) is implemented and afterwards, the signal is directed to the transmit-receive coupler (TRC), where the signal is guided towards the on-chip antenna.

The signal received at each antenna is fed to the biomimetic coupling network (BMC) through the transmit-receive coupler. Thereafter, the received signal is amplified by a low-noise amplifier (LNA) and subsequently mixed down with the LO signal to the base band (intermediate frequency, IF).

The realized MMIC is depicted in Fig. 6. It occupies a chip area of less than $3\,\text{mm}^2$ with a length of $2.46\,\text{mm}$ and a width of $1.21\,\text{mm}$ and is realized in an $130\,\text{nm}$ SiGe-BiCMOS technology with an $f_T/f_{\max}$ of $300\,\text{GHz}/500\,\text{GHz}$. Special emphasis was placed on routing the two channels of the MMIC symmetrically. Additionally, the antennas and the bond connections were placed on different sides of the MMIC so that the mutual interference between them is minimized. The tight design of the MMIC allows for cascading, e. g., to built up larger radar systems.

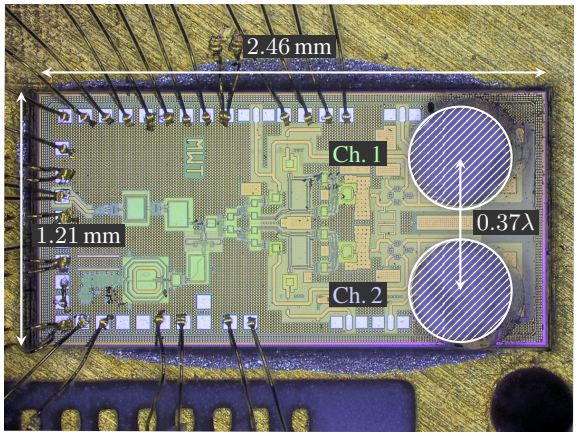

Fig. 6. Chip photo of the bonded two-channel radar sensor with its outer dimensions. The chip is equipped with two dielectric resonator antennas (DRAs) placed on top of the on-chip patch antennas.

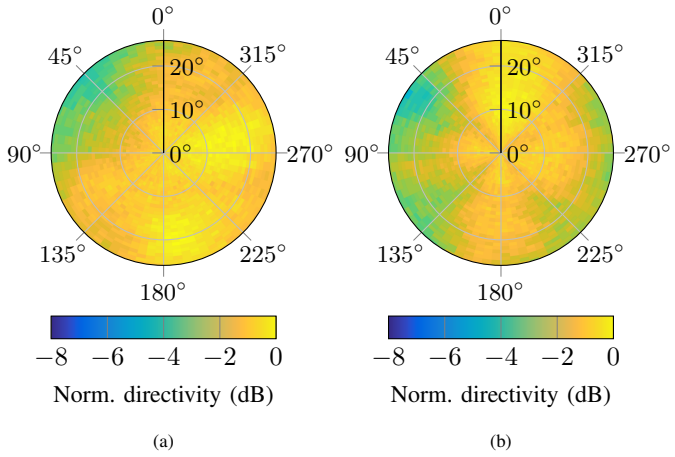

Fig. 7. Measured 3D-radiation patterns of the on-chip antennas of (a) channel 1 and (b) channel 2 at 150 GHz, respectively. The scanning plane of the radar (E-plane) is oriented vertically, the H-plane horizontally.

B. Integrated On-Chip Antennas and Biomimetic Coupling

The integrated antennas of the MMIC are designed according to the work in [4], [27], [28] and are composed of two parts. The first part is a shorted $\lambda/4$-patch with a dimension of $220\,\mu\text{m} \times 180\,\mu\text{m}$, realized on the topmost layer of the back-end of line (BEOL) of the semiconductor process. Two of these patches are spaced at a distance of $d = 470\,\mu\text{m} \approx \lambda/4$. The second component is a dielectric resonator antenna (DRA) with a diameter of $515\,\mu\text{m}$ and a height of $700\,\mu\text{m}$ placed on top of each of the structures to couple out the strong electric fields generated at the open end of the patch resulting in a spacing of 0.37λ (see Fig. 6). The measured 3D-radiation patterns of both antennas at 150 GHz are given in Fig. 7. The simulated maximum gain of each antenna is 3.8 dBi at a 3 dB-beamwidth of 90°.

By using the method presented in Section II-A a BMAA was built. The target design parameters were $\eta = 3$ and $L_{\text{out}} = -9.5\,\text{dB}$. Thus, the aperture is enlarged in boresight direction by a factor of 3, resulting in a total aperture size of $d_{\text{bio}} \approx \lambda$. The biomimetic coupling network is designed

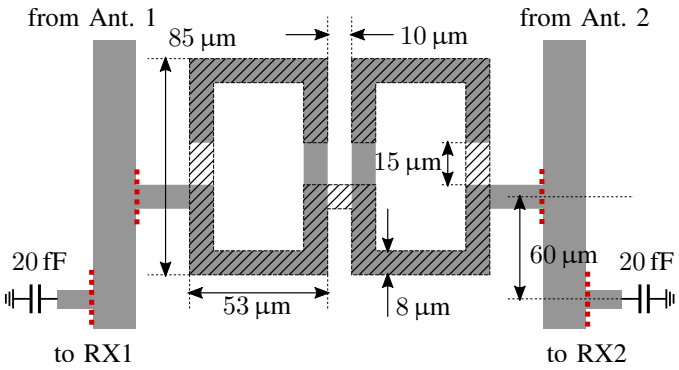

Fig. 8. Layout of the biomimetic coupling network (BMC) consisting of two transformers realized on the MMIC. Structures on the topmost layer are displayed in gray, structures located one layer below are shown in hatched. The BMC can be disconnected by cutting at the dotted red lines.

according to the generalized model presented in [18] and is implemented in the receiving path of the MMIC. A sketch of the layout of the realized biomimetic coupling network is depicted in Fig. 8. It consists of two vertically stacked microstrip line transformers on the two topmost metal layers of the semiconductor process. The antenna Y-parameters as the starting point of the design process were extracted from full-wave simulations. The required transmission characteristics of the biomimetic coupling network, calculated by the design process, are then realized by adjusting the transmission factors from Ant. 1 to RX1 and from Ant. 1 to RX2, respectively. In order to realize the desired phase gain of $\eta = 3$ for the presented antennas, the difference Δ in magnitude and phase of these transmission factors need to fulfill $|\Delta| = -2.4\,\text{dB}$ and $\arg(\Delta) = 178.9°$. The complete biomimetic coupling network was optimized by full-wave simulations and the two transformers were additionally measured on a separate breakout chip in order to confirm the simulations. A matching network using a shunt MIM-capacitor is realized and placed at a distance of $60\,\mu\text{m}$ from the transformers towards the receivers. The coupling network is designed in a way that it can be disconnected by cutting the transformer feed lines as well as the matching stubs e.g. with the focused ion beam (FIB) technology. This allows to identify the properties of MMICs equipped with BMAAs by comparing them to identical MMICs without biomimetic coupling.

C. MIMO System Concept and Biomimetic MIMO

Since the presented MMIC incorporates two transmitters and two receivers, a minimal MIMO system can be built up. The orthogonality of the transmitting signals is achieved by means of a time multiplexing by switching the power amplifier (PA) in the TX path on and off. A measured suppression of the TX signal of larger than 27 dB is achieved in the frequency band of interest by switching off the PA.

The redundant element in the virtual aperture—due to the monostatic configuration of the MMIC—is split into two separate elements by the biomimetic MIMO principle described in Section II-B. Thus, the overall aperture consists of four individual elements and is theoretically capable of separating

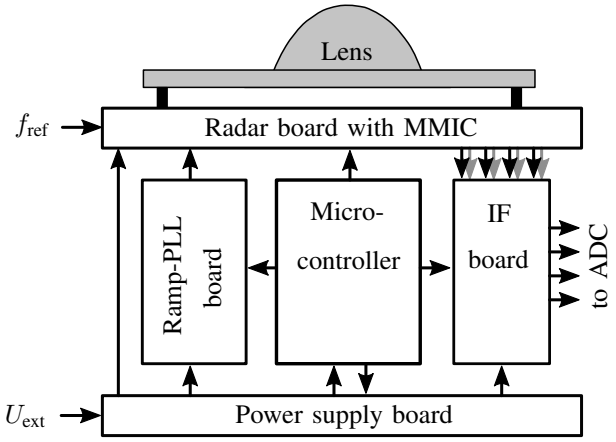

Fig. 9. Block diagram of the modular radar system. The radar MMIC is mounted on the radar board.

TABLE I
RADAR MODULATION PARAMETERS

Ramp duration T_{up}	100 µs
Ramp repetition time T_r	150 µs
Center frequency f_c	152.92 GHz
RF bandwidth B	8.24 GHz
Number of ramps N_r	512

three targets in the angular domain. Due to its increased phase progression, the size of the BMAA aperture also appears to be enlarged depending on the value of the phase gain [20] compared to the conventional array. In boresight direction the presented MIMO system therefore exhibits a total array size of $D=(\eta+1)d$ where $d=0.37\lambda$ is the physical element separation on the realized MMIC. Due to a phase gain of $\eta=3$, the resulting MIMO aperture in this work is doubled in size compared to the conventional MIMO aperture.

The theoretical diffraction limit for an antenna array to distinguish between two targets is given by the Rayleigh criterion [29]

$$\Delta\theta = \frac{\lambda}{D} = \frac{\lambda}{(\eta+1)d}\,, \tag{12}$$

where D is the total aperture size. With a designed phase gain of $\eta=3$ for the presented MMIC a theoretical angular resolution of $\Delta\theta=38.7°$ is possible compared to $\Delta\theta=154.8°$ and $\Delta\theta=77.4°$ for the conventional SIMO and MIMO array, respectively.

The application of BMAAs in a radar system is subject to a fundamental trade-off, as already stated in Section II-A. Any increase in angle estimation performance will reduce the SNR by L_{out}, which in turn leads to a reduced range of the radar system. In general, due to the R^{-4} dependency of the radar equation, the following relation can be used to estimate the reduction in maximum range R_{max} of the radar system assuming a required minimum receive power at the receiver:

$$R_{\text{max,BMAA}} = \sqrt[4]{L_{\text{out}}}R_{\text{max,conv}}\,. \tag{13}$$

In the case under consideration, the reduction of the maximum range R_{max} for a designed L_{out}=−9.5 dB is about 42% when applying BMAAs instead of a conventional array.

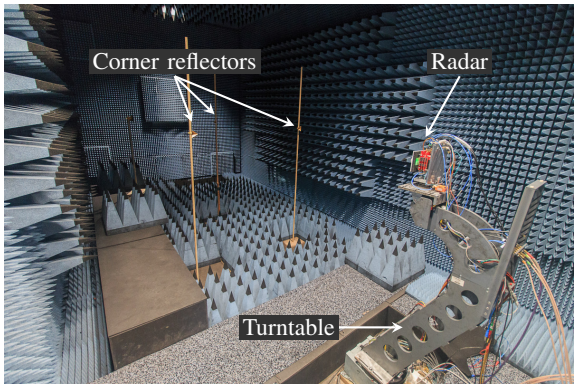

Fig. 10. Photograph of the measurement setup in an anechoic chamber used to characterize the radar system.

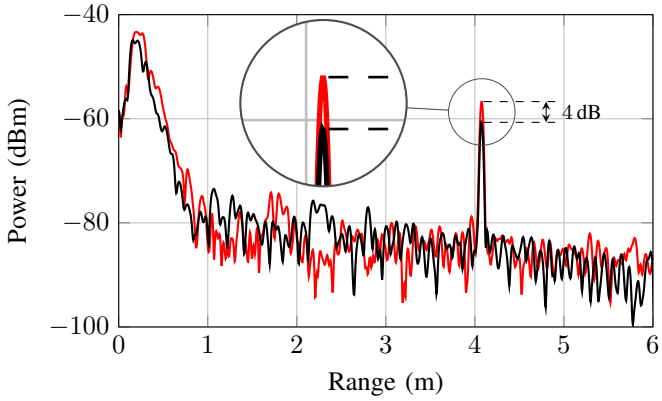

Fig. 11. Measured power range profile for one target at $\theta=0°$ using the conventional (——) and the biomimetic (——) radar board. The signals of all four virtual channels were integrated non-coherently.

IV. RADAR MEASUREMENTS

A. Measurement Setup

The developed MMIC was used in a modular radar system consisting of five stacked PCBs, each providing a specific purpose. A block diagram of the system is given in Fig. 9. The radar MMIC presented in Section III is mounted on the radar board, and a cylindrical lens is placed over the board to focus the antenna beam in the elevation plane while leaving the beam in the azimuth plane unaltered. The resulting field-of-view (FOV) in the azimuth plane is ±35°. The FMCW frequency ramp is generated with an off-the-shelf PLL with external VCO on the ramp-PLL board. The signals received by the radar are directed to the IF board, where the signals are filtered and amplified by a factor of up to 60 dB and subsequently forwarded to an external Analog-to-Digital Converter (ADC). A microcontroller is used to program the modulation settings, modify the IF signal conditioning parameters, and control the radar MMIC. Two radar boards were built up in this work, one of which is carrying the unmodified MMIC (subsequently called *biomimetic radar board*) while the other one carries an MMIC with disconnected biomimetic coupling network (subsequently called *conventional radar board*).

The radar modulation parameters used in the measurements are given in Tab. I. All radar measurements were conducted

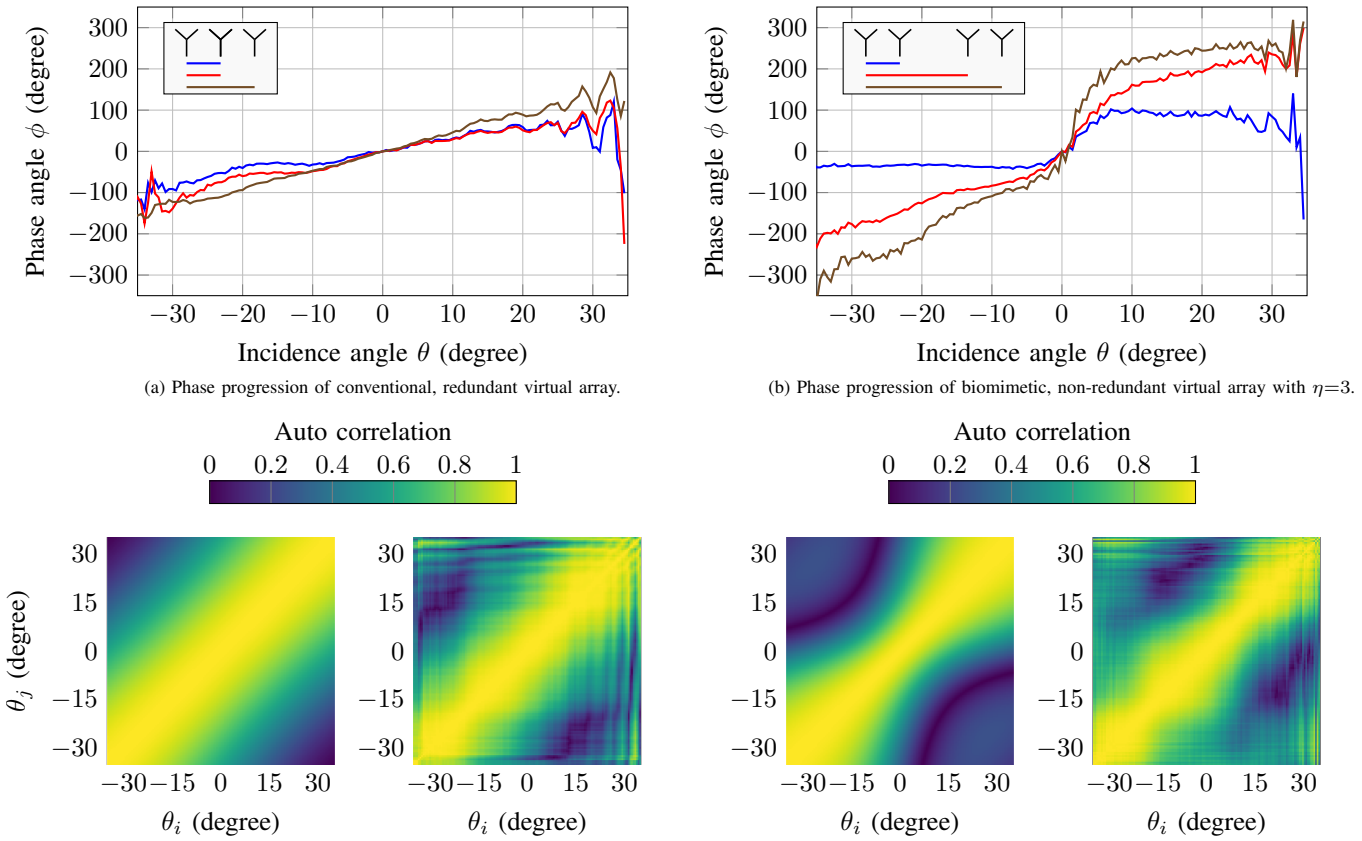

(a) Phase progression of conventional, redundant virtual array.

(b) Phase progression of biomimetic, non-redundant virtual array with η=3.

(c) Sim. (left) and meas. (right) AF of conventional, redundant virtual array.

(d) Sim. (left) and meas. (right) AF of biomimetic, non-redundant virtual array.

Fig. 12. Measured phase progressions normalized to the first array element for (a) the conventional and (b) the biomimetic aperture and simumlated and measured absolute value of the ambiguity function (AF) for (c) the conventional and (d) the biomimetic aperture.

in an anechoic chamber while the radar stack was mounted on a turntable, see Fig. 10. Corner reflectors with different radar-cross-sections (RCS) placed in the far field of the radar served as targets.

TABLE II
NORMALIZED OUTPUT POWER LEVEL L_{OUT} OF EVERY VIRTUAL CHANNEL FOR A TARGET AT $\theta = 0°$

	chan. 1	chan. 2	chan. 3	chan. 4
L_{out}	−0.4 dB	−6.4 dB	−12.3 dB	−5.9 dB

B. Radar Measurements

The system performance and the angular estimation performance are evaluated by radar measurements using a single target at a distance of around 4 m at boresight ($\theta = 0°$). Fig. 11 shows the power range profile of both radar boards under test. The IF signals of all four virtual channels are integrated non-coherently. It can be noticed that the overall shape of the graphs and the noise floor is comparable among the two boards whereas the biomimetic radar board shows a 4 dB lower target power level. However, the reduction of the power level is lower compared to the designed L_{out} value of −9.5 dB. Tab. II lists the L_{out} values for each individual virtual channel determined by the target peak difference of the measurements with the biomimetic and the conventional radar board. While in theory the normalized output power is the same for every virtual channel, deviations can be found in the measurements. This is due to fabrication tolerances like e.g. the placement of the DRAs on the MMICs and parasitic influences of the measurement setup. By integrating the values of Tab. II, the measured reduction of 4 dB is obtained. Referring to the weakest of the measured virtual channels, the maximum range R_{max} of the biomimetic radar board according to (13) is reduced by 50% compared to the conventional radar board.

In a next step, the radar was rotated around its axis with the target fixed at 0°. A radar measurement was performed for every angle in the range $\theta = -35°...35°$ with a step size of 0.5°. For each measurement and for every virtual channel the phase at the target location was extracted from the power range profile, and the phase progression between the respective virtual channels was calculated. Figs. 12(a) and 12(b) show the measured phase progressions normalized to the first virtual array element using the conventional and the biomimetic radar board, respectively. The effect of the biomimetic coupling can clearly be noticed as the single curves in Fig. 12(b) show a significantly steeper slope in the vicinity of boresight. It can also be noticed that Fig. 12(a) shows three curves but two of them lie almost on top of each other. This means, a redundant element is present for the conventional radar board

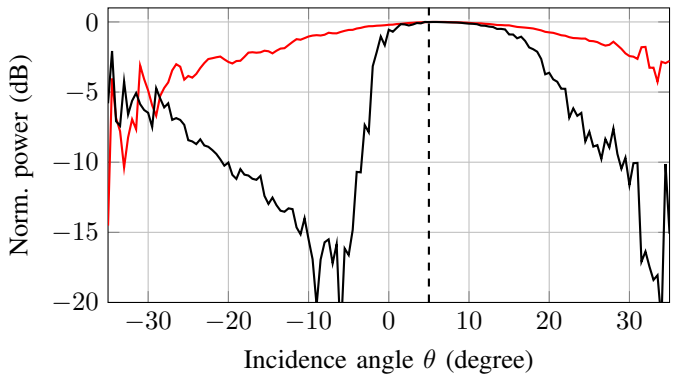

Fig. 13. Measured angular estimation performance of the conventional (——) and the biomimetic (——) MIMO radar system for one target at $\theta = 5°$. The true DOA is marked with a dashed line.

as predicted in Section II. In Fig. 12(b), this redundancy is no more visible as all three curves show a unique course and are clearly separable. Thus, the redundancy of the monostatic MIMO radar has been eliminated by using the biomimetic radar board.

From the measured phase progressions, the ambiguity diagrams for both radar systems under test were calculated according to (11) and are depicted in Figs. 12(c) and 12(d). Whereas the conventional radar board shows a constant width of the main beam, a clear constriction can be noticed for the biomimetic radar board, especially for $\theta > 0°$. This originates from the steeper phase progression and is leading to a smaller lobe in the angle estimation. The experimental results are in good agreement with the theoretical findings in Fig. 4.

For a target placed at an angle of 5° at a distance of 3 m to the radar, the angle estimation spectra are depicted in Fig. 13 for the conventional and the biomimetic radar. A maximum likelihood (ML) method was used for the angle estimation in which the measured data is correlated with a prerecorded calibration vector of all incidence angles θ and normalized to 0 dB. The significantly narrower lobe of the ambiguity plot can also be noticed here, leading to a more accurate angle estimation. A statistical study on the angle estimation accuracy by performing 100 measurements with only one transmitter being active (SIMO case) was already presented in [26] showing an improvement in angular accuracy of around a factor of 2 for a phase gain of $\eta = 4$.

V. Conclusion

This contribution proposed biomimetic MIMO as a fundamentally new MIMO principle based on the concept of biomimetic antenna arrays to overcome the problem of redundant elements in monostatic MIMO systems. The new MIMO principle was applied to an ultra-compact monostatic radar based on an MMIC in the 150 GHz range with two transmit and receive channels occupying a chip area of 3 mm^2 only. Radar measurements utilizing the presented MMIC verified the working principle of the new MIMO concept. A virtual aperture consisting of four unique antenna positions and an equivalent total size of around 1.5λ was obtained. The presented concept is not limited to monostatic setups but also holds for bistatic MIMO radars where the transmitting and receiving antennas are spaced identically.

Appendix
Derivation of formula for L_{OUT}

The normalized output power L_{out} of the biomimetic antenna array (BMAA) is defined as [18]

$$L_{\mathrm{out}} = \left| \frac{u_{i,\mathrm{BMAA}}}{u_{i,\mathrm{conv.}}} \right|^2 \quad \text{with } i = 1, 2\,, \tag{14}$$

where $u_{i,\mathrm{BMAA}}$ and $u_{i,\mathrm{conv.}}$ are the voltages at the antenna system output for the biomimetic and the conventional antenna array, respectively, and i indicates the corresponding antenna port. The two voltages have been derived in [18] as

$$u_{i,\mathrm{BMAA}} = \frac{\pm \mathrm{j} A_0 \sin\alpha}{Y_{11} - Y_{12} + G_L} + \frac{A_0 \cos\alpha}{Y_{11} + Y_{12} + G_L + G_C + \mathrm{j}B_C} \tag{15}$$

$$u_{i,\mathrm{conv.}} = \frac{\pm \mathrm{j} A_0 \sin\alpha}{Y_{11} - Y_{12} + G_L} + \frac{A_0 \cos\alpha}{Y_{11} + Y_{12} + G_L}\,, \tag{16}$$

depending on the antenna Y-parameters (Y_{11}, Y_{12}), the load (G_L), and the lumped elements of the coupling network (G_C, B_C). The coupling network elements G_C and B_C are not present for the conventional antenna array, i. e., $G_C = B_C = 0$. Inserting into (14), rearranging, and introducing the variable z as

$$z = \eta + \mathrm{j}\xi = \frac{Y_{11} + Y_{12} + G_L + G_C + \mathrm{j}B_C}{Y_{11} - Y_{12} + G_L}\,, \tag{17}$$

the following equation for L_{out} is derived:

$$L_{\mathrm{out}} = \left| \frac{\frac{1}{z} \pm \mathrm{j}\tan\alpha}{1 + \mathrm{j}\tan\alpha} \right|^2 = \left| \frac{1 \pm \mathrm{j}\,(\eta + \mathrm{j}\xi)\tan\alpha}{\eta + \mathrm{j}\left(\xi + (\eta + \mathrm{j}\xi)\tan\alpha\right)} \right|^2 . \tag{18}$$

References

[1] M. Schröter, T. Rosenbaum, P. Chevalier, B. Heinemann, S. P. Voinigescu, E. Preisler, J. Böck, and A. Mukherjee, "SiGe HBT Technology: Future Trends and TCAD-Based Roadmap," *Proc. of the IEEE*, vol. 105, no. 6, pp. 1068–1086, Jun. 2017.

[2] S. P. Voinigescu, S. Shopov, J. Bateman, H. Farooq, J. Hoffman, and K. Vasilakopoulos, "Silicon Millimeter-Wave, Terahertz, and High-Speed Fiber-Optic Device and Benchmark Circuit Scaling Through the 2030 ITRS Horizon," *Proc. of the IEEE*, vol. 105, no. 6, pp. 1087–1104, Jun. 2017.

[3] I. Sarkas, J. Hasch, A. Balteanu, and S. Voinigescu, "A Fundamental Frequency 120-GHz SiGe BiCMOS Distance Sensor With Integrated Antenna," *IEEE Trans. Microw. Theory Techn.*, vol. 60, no. 3, pp. 795–812, Mar. 2012.

[4] M. Hitzler, S. Saulig, L. Boehm, W. Mayer, W. Winkler, N. Uddin, and C. Waldschmidt, "Ultracompact 160-GHz FMCW Radar MMIC With Fully Integrated Offset Synthesizer," *IEEE Trans. Microw. Theory Techn.*, vol. 65, no. 5, pp. 1682–1691, May 2017.

[5] A. Mostajeran, A. Cathelin, and E. Afshari, "A 170-GHz Fully Integrated Single-Chip FMCW Imaging Radar with 3-D Imaging Capability," *IEEE J. Solid-State Circuits*, vol. 52, no. 10, pp. 2721–2734, Oct. 2017.

[6] S. Thomas, C. Bredendiek, T. Jaeschke, F. Vogelsang, and N. Pohl, "A Compact, Energy-Efficient 240 GHz FMCW Radar Sensor with High Modulation Bandwidth," in *German Microw. Conf. (GeMiC)*, Bochum, Mar. 2016, pp. 397–400.

[7] H. J. Ng, M. Kucharski, W. Ahmad, and D. Kissinger, "Multi-Purpose Fully Differential 61- and 122-GHz Radar Transceivers for Scalable MIMO Sensor Platforms," *IEEE J. Solid-State Circuits*, vol. 52, no. 9, pp. 2242–2255, Sep. 2017.

[8] A. Mostajeran, S. M. Naghavi, M. Emadi, S. Samala, B. P. Ginsburg, M. Aseeri, and E. Afshari, "A High-Resolution 220-GHz Ultra-Wideband Fully Integrated ISAR Imaging System," *IEEE Trans. Microw. Theory Techn.*, vol. 67, no. 1, pp. 429–442, Jan. 2019.

[9] M. G. Girma, J. Hasch, I. Sarkas, S. P. Voinigescu, and T. Zwick, "122 GHz Radar Sensor based on a Monostatic SiGe-BiCMOS IC with an On-Chip Antenna," in *7th Europ. Microw. Integ. Circuits Conf.*, Amsterdam, Oct. 2012, pp. 357–360.

[10] E. Öztürk, D. Genschow, U. Yodprasit, B. Yilmaz, D. Kissinger, W. Debski, and W. Winkler, "A 120 GHz SiGe BiCMOS Monostatic Transceiver for Radar Applications," in *13th Europ. Microw. Integ. Circuits Conf. (EuMIC)*, Madrid, Sep. 2018, pp. 41–44.

[11] M. Hitzler, P. Grüner, L. Boehm, W. Mayer, and C. Waldschmidt, "On Monostatic and Bistatic System Concepts for mm-Wave Radar MMICs," *IEEE Trans. Microw. Theory Techn.*, vol. 66, no. 9, pp. 4204–4215, Sep. 2018.

[12] S. Shopov, M. G. Girma, J. Hasch, N. Cahoon, and S. P. Voinigescu, "Ultralow-Power Radar Sensors for Ambient Sensing in the V-Band," *IEEE Trans. Microw. Theory Techn.*, vol. 65, no. 12, pp. 5401–5410, Dec. 2017.

[13] E. Öztürk, D. Genschow, U. Yodprasit, B. Yilmaz, D. Kissinger, W. Debski, and W. Winkler, "A 60 GHz SiGe BiCMOS Monostatic Transceiver for Radar Applications," in *IEEE MTT-S Int. Microw. Symp. (IMS)*, Honolulu, HI, Jun. 2017, pp. 1408–1411.

[14] M. G. Girma, M. Gonser, A. Frischen, J. Hasch, Y. Sun, and T. Zwick, "122 GHz single-chip dual-channel SMD radar sensor with on-chip antennas for distance and angle measurements," *Int. J. of Microw. and Wireless Techn.*, vol. 7, no. 3-4, pp. 407–414, Jun. 2015.

[15] H. J. Ng and D. Kissinger, "Highly Miniaturized 120-GHz SIMO and MIMO Radar Sensor With On-Chip Folded Dipole Antennas for Range and Angular Measurements," *IEEE Trans. Microw. Theory Techn.*, vol. 66, no. 6, pp. 2592–2603, Jun. 2018.

[16] R. N. Miles, D. Robert, and R. R. Hoy, "Mechanically coupled ears for directional hearing in the parasitoid fly Ormia ochracea," *The J. of the Acoust. Soc. of Amer.*, vol. 98, no. 6, pp. 3059–3070, Dec. 1995.

[17] A. R. Masoumi, Y. Yusuf, and N. Behdad, "Biomimetic Antenna Arrays Based on the Directional Hearing Mechanism of the Parasitoid Fly Ormia Ochracea," *IEEE Trans. Antennas Propag.*, vol. 61, no. 5, pp. 2500–2510, May 2013.

[18] P. Grüner, T. Chaloun, and C. Waldschmidt, "A Generalized Model for Two-Element Biomimetic Antenna Arrays," *IEEE Trans. Antennas Propag.*, vol. 67, no. 3, pp. 1630–1639, Mar. 2019.

[19] M. R. Nikkhah, K. Ghaemi, and N. Behdad, "An Electronically Tunable Biomimetic Antenna Array," *IEEE Trans. Antennas Propag.*, vol. 66, no. 3, pp. 1248–1257, Mar. 2018.

[20] P. Grüner, T. Chaloun, and C. Waldschmidt, "Enhanced Angle Estimation Accuracy of Ultra Compact Radars Inspired by a Biomimetic Approach," in *IEEE MTT-S Int. Microw. Symp. (IMS)*, Honolulu, HI, Jun. 2017, pp. 1425–1428.

[21] J. Li and P. Stoica, Eds., *MIMO Radar Signal Processing*. Hoboken, NJ: J. Wiley & Sons, 2009.

[22] A. R. Masoumi and N. Behdad, "An Improved Architecture for Two-Element Biomimetic Antenna Arrays," *IEEE Trans. Antennas Propag.*, vol. 61, no. 12, pp. 6224–6228, Dec. 2013.

[23] P. Grüner, S. Nguyen, T. Chaloun, and C. Waldschmidt, "Enhancing Angle Estimation for Off-Boresight Targets Using Biomimetic Antenna Arrays," in *48th Europ. Microw. Conf. (EuMC)*, Madrid, Sep. 2018, pp. 1377–1380.

[24] F. C. Robey, S. Coutts, D. Weikle, J. C. McHarg, and K. Cuomo, "MIMO Radar Theory and Experimental Results," in *Conf. Rec. of the Thirty-Eighth Asilomar Conf. on Signals, Syst. and Comp.*, Pacific Grove, CA, Nov. 2004, pp. 300–304.

[25] M. Eric, A. Zejak, and M. Obradovic, "Ambiguity characterization of arbitrary antenna array: type I ambiguity," in *IEEE 5th Int. Symp. on Spread Spectrum Techn. and Applicat.*, vol. 2, Sun City, South Africa, Sep. 1998, pp. 399–403.

[26] P. Grüner, T. Chaloun, and C. Waldschmidt, "Enhancing Angle Estimation Accuracy of Ultra Compact Two-Channel Radar MMICs at 160 GHz Using a Biomimetic Antenna Array," in *IEEE MTT-S Int. Microw. Symp. (IMS)*, Boston, Mass., Jun. 2019, pp. 305–308.

[27] M. Hitzler and C. Waldschmidt, "Design and Characterization Concepts of a Broadband Chip-Integrated Antenna," in *44th Europ. Microw. Conf. (EuMC)*, Rome, Oct. 2014, pp. 96–99.

[28] J. Hasch, U. Wostradowski, S. Gaier, and T. Hansen, "77 GHz Radar Transceiver with Dual Integrated Antenna Elements," in *German Microw. Conf. (GeMiC)*, Berlin, Mar. 2010, pp. 280–283.

[29] H. L. Van Trees, *Optimum Array Processing*, ser. Detection, estimation, and modulation theory. John Wiley & Sons, Ltd, 2002, no. 4.

Patrik Grüner (S'15) received the M.Sc. degree in electrical engineering from Ulm University, Ulm, Germany, in 2015, where he is currently pursuing the Ph.D. degree.

In 2015, he joined the Institute of Microwave Engineering (MWT), Ulm University. His current research interests include compact FMCW radar sensors and biomimetic antenna systems both in the microwave and mm-wave range.

Mr. Grüner was a recipient of the ARGUS Science Award in 2013 and the Best Paper Award of the 2013 International Workshop on Antenna Technology.

Martin Geiger received the M.Sc. degree from Ulm University, Ulm, Germany, in 2015, where he is currently pursuing the Ph.D. degree.

In 2016, he joined the Institute of Microwave Engineering, Ulm University. His current research interests include novel radar sensor concepts with flexible antennas, dielectric waveguides, and MMIC interconnects, all at mm-wave frequencies.

Mr. Geiger was a recipient of the Best Student Paper Award of the 2018 International Microwave Symposium.

Christian Waldschmidt (S'01-M'05-SM'13) received the Dipl.-Ing. (M.S.E.E.) and the Dr.-Ing. (Ph.D.E.E.) degrees from the University Karlsruhe (TH), Karlsruhe, Germany, in 2001 and 2004, respectively. From 2001 to 2004 he was a Research Assistant at the Institut für Höchstfrequenztechnik and Elektronik (IHE), Universität Karlsruhe (TH), Germany. Since 2004 he has been with Robert Bosch GmbH, in the business units Corporate Research and Chassis Systems. He was heading different research and development teams in microwave engineering, RF-sensing, and automotive radar.

In 2013 Christian Waldschmidt returned to academia. He was appointed as the Director of the Institute of Microwave Engineering at University Ulm, Germany, as full professor. The research topics focus on radar and RF-sensing, mm-wave and submillimeter-wave engineering, antennas and antenna arrays, RF and array signal processing. He authored or coauthored over 200 scientific publications and more than 20 patents.

He is member of the executive committee board of the German MTT/AP joint chapter, and member of the German Information Technology Society (ITG). He served as chair of the IEEE MTT-27 Technical Committee on wireless enabled automotive and vehicular applications. He was a two-time TPC chair and general chair of the IEEE MTT International Conference on Microwaves for Intelligent Mobility. Since 2018, Christian Waldschmidt serves as associate editor for IEEE MTT Microwave Wireless Components Letters (MWCL). He is a reviewer for multiple IEEE transactions and many IEEE conferences in the field of microwaves. Christian Waldschmidt was co-recipient of 11 best paper awards since 2014.